

Antitumor Agents. 1. Synthesis, Biological Evaluation, and Molecular Modeling of 5*H*-Pyrido[3,2-*a*]phenoxazin-5-one, a Compound with Potent Antiproliferative Activity

Adele Bolognese,^{*,†} Gaetano Correale,[†] Michele Manfra,[†] Antonio Lavecchia,[‡] Orazio Mazzoni,[‡] Ettore Novellino,[‡] Vincenzo Barone,[§] Alessandra Pani,^{||} Enzo Tramontano,^{||} Paolo La Colla,^{||} Chiara Murgioni,^{||} Ilaria Serra,^{||} Giovanna Setzu,^{||} and Roberta Loddo^{||}

Dipartimento di Chimica Organica e Biochimica and Dipartimento di Chimica, Università di Napoli "Federico II", Via Cynthia 6, Monte Sant'Angelo, I-80126 Napoli, Italy, Dipartimento di Chimica Farmaceutica e Tossicologica, Università di Napoli "Federico II", Via D. Montesano 49, 80131 Napoli, Italy, and Dipartimento di Biologia Sperimentale, Sezione di Microbiologia, Università di Cagliari, Cittadella Universitaria SS 554, I-09042 Monserrato (Cagliari), Italy

Received April 19, 2002

The iminoquinone is an important moiety of a large number of antineoplastic drugs and plays a significant role in the nucleus of actinomycins, powerful, highly toxic, natural antibiotics that target DNA as intercalating agents. A series of polycyclic iminoquinonic compounds, 2-amino-3*H*-phenoxazin-3-one (**1**), 2-amino-1,9-diacetyl-3*H*-phenoxazin-3-one (**2**), 2-acetylamino-3*H*-phenoxazin-3-one (**3**), 3*H*-phenoxazin-3-one (**4**), 5*H*-pyrido[3,2-*a*]phenoxazin-5-one (**5**), and 5*H*-pyrido[3,2-*a*]phenothiazin-5-one (**6**), strictly related to the actinomycin chromophore, were synthesized for developing new anticancer intercalating drugs. The antiproliferative activity of these compounds, evaluated against representative human liquid and solid neoplastic cell lines, showed that **5** and its isoster **6** were the most active compounds inhibiting cell proliferation in a submicromolar range. Compound **5** was also evaluated against KB subclones (KB^{MDR}, KB^{7D}, and KB^{V20C}), which overexpress the MDR1/P-glycoprotein drug efflux pump responsible for drug resistance. All the above KB subclones did not show altered sensitivity to the antiproliferative activity of **5**. UV-vis and ¹H NMR spectroscopy experiments support the phenoxazinone **5**/DNA binding. Molecular mechanics methods were used to build a three-dimensional model of the **5**/[d(GAAGCTTC)]₂ complex. Electrostatic interactions between the hydrogen of the positively charged pyridine nitrogen of **5** and the negatively charged oxygen atoms (O4' and O5') of the cytosine C5 residue together with stacking forces contribute to the high antiproliferative activity. The metal(II)-assisted synthesis procedure of **5** is described, and the formation mechanism is proposed.

Introduction

One of the cytostatic mechanisms of coplanar polycyclic compounds is their intercalation with human DNA, which determines enzymatic blocking and reading errors during the replication process. If the compounds have three to four coplanar rings, they give the optimal intercalation.

Natural phenoxazinones, containing a tricyclic iminoquinone system, are present among the ommochromes (xanthommatin and dihydroxanthommatin) and ommins^{1,2} (pigments responsible for the skin and eye colors of invertebrates), among the cinnabarins³ (wood-rotting fungi metabolites), and among the actinomycins (powerful antibiotics produced by certain species of *Streptomyces*) (Chart 1).

Actinomycin D (AMD), obtained from *Streptomyces parvulus*, is known to be the best DNA intercalating agent⁴ in nature, but its clinical application is limited

because of the side effects associated with myelosuppression and cardiotoxicity. The powerful damaging effect on DNA transcription has been correlated to the formation of a stable DNA/drug complex, where the phenoxazinone moiety is responsible for the intercalation between specific base pairs. X-ray investigations performed on stable crystallized complexes^{5–8} have shown that AMD intercalates between the middle 5'-GC-3' base pairs. The 2-amino group on the phenoxazinone system is involved in hydrogen bonding to the O4' and/or O5' of the cytosine C5 residue, and its substitution with a chlorine atom is reported to be detrimental for activity.⁹ The peptide chains arrange themselves along the minor groove of the DNA helix.

In light of the reported considerations and with the aim of obtaining active and anticancer drugs with low toxicity, the unsubstituted 2-amino tricyclic system of AMD, the phenoxazinone **1**,¹⁰ was used as the lead compound and subjected to structural modifications (Chart 2). The peptide chains in positions 1 and 9 of AMD were replaced with acetyl groups to mimic the peptide carbonyl groups (**2**),² and the nucleophilic character of 2-amino substituent was changed by acetylation (**3**)¹⁰ to investigate the crucial role of the 2-amino group in the intercalation process. Phenoxazinone **4**¹⁰

* To whom correspondence should be addressed. Phone: ++39 081 674121. Fax: ++39 081 674393. E-mail: bologne@unina.it.

[†] Dipartimento di Chimica Organica e Biochimica, Università di Napoli "Federico II".

[‡] Dipartimento di Chimica Farmaceutica e Tossicologica, Università di Napoli "Federico II".

[§] Dipartimento di Chimica, Università di Napoli "Federico II".

^{||} Università di Cagliari.

Chart 1

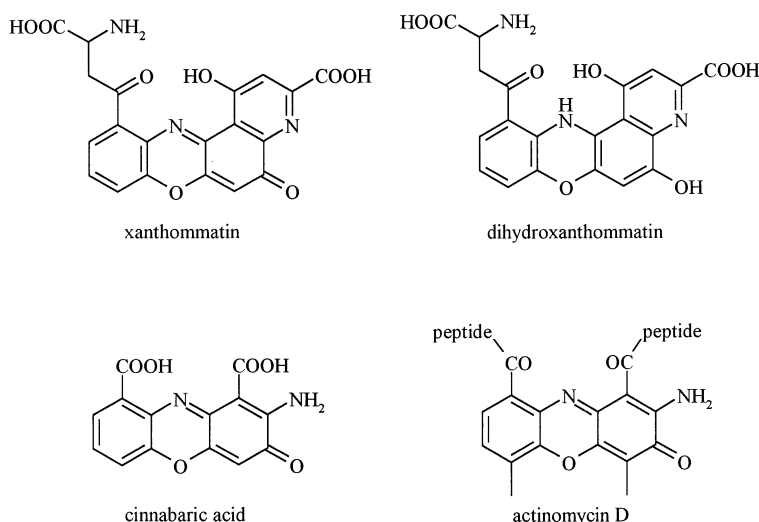
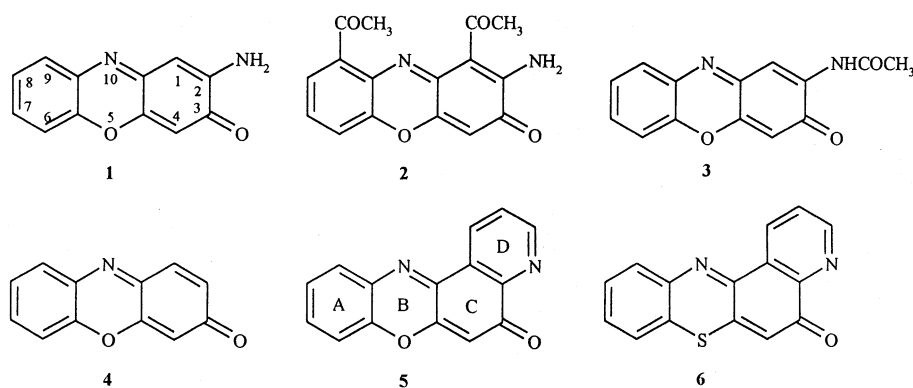
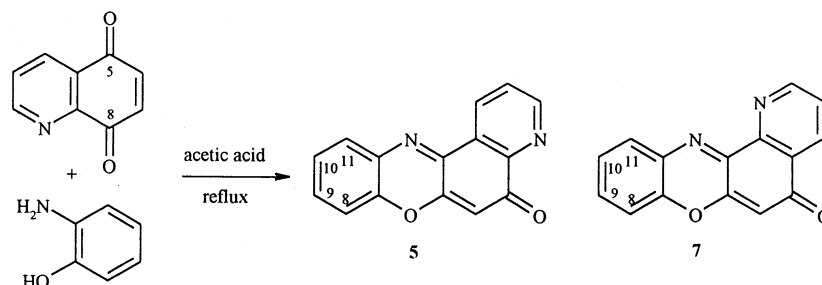


Chart 2



Scheme 1



was synthesized to test the activity of the simple iminoquinone nucleus.

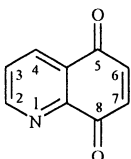
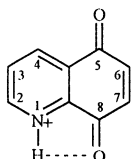
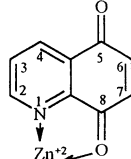
The biological activity decreased according to $4 < 3 < 1 < 2$, suggesting the significant role played by the 2-amino function, so the pyridine-fused analogue **5**¹¹ was prepared. The isosteric pyridophenothiazinone **6** was also synthesized¹² by substitution of the oxygen bridge with a larger and more lipophilic sulfur atom.

The present paper describes the design, biological evaluation, and structure–activity relationships (SARs) of phenoxazinones **1–4**, pyridophenoxazinone **5**, and pyridophenothiazinone **6**. The high activity of compound **5** induced us to investigate its binding to DNA through UV–vis measurements and ¹H NMR studies. The 5/[d(GAAGCTTC)]₂ complex was subjected to molecular dynamics (MD) simulations by using explicit solvent molecules and particle mesh Ewald (PME) treatment¹³ of the electrostatic force.

Results and Discussion

Chemistry. Phenoxazinones **1–5** and phenothiazinone **6** were prepared according to the reported procedures.^{2,10–12} According to ref 12, 5H-pyrido[3,2-a]phenoxazin-5-one (**5**) is formed in very small amounts together with 5H-pyrido[2,3-a]phenoxazin-5-one (**7**) (2% and 7%, respectively). Owing to our interest in obtaining **5**, an investigation on the formation of pyridophenoxazinones was accomplished to improve the reaction yields and to enhance the selectivity. In the course of these experiments, 2-aminophenol and quinolin-5,8-dione were used and acetic acid was found to be the best solvent (Scheme 1). Nevertheless, the reaction course was unsatisfactory; the **5** + **7** yield was about 15% (**5**/**7** ratio of 1:4), and the main products present in the reaction mixtures were triphenodioxazine, 2-amino- and 2-hydroxyphenoxazin-3-one, and unidentified black materials.

Table 1. HOMO and LUMO Orbital Coefficients and Charge Density of Nonprotonated, N-Protonated, and Zn(II)-Complexed Quinolin-5,8-dione Calculated by *ab Initio* Methods

									
	orbital coefficient, nonprotonated (eV)		charge density (e ⁻)	orbital coefficient, N-protonated (eV)		charge density (e ⁻)	orbital coefficient, Zn-complexed (eV)		charge density (e ⁻)
HOMO	LUMO	HOMO		LUMO	HOMO		LUMO		
C ₅	-0.151 53	-0.302 22	0.4154	-0.198 83	-0.082 21	0.4339	-0.013 91	-0.198 27	0.4241
C ₈	-0.154 38	0.278 06	0.4404	-0.151 86	0.229 23	0.4795	0.186 78	0.383 09	0.4911
C ₆	0.217 78	-0.458 91	0.0139	0.465 79	-0.185 20	0.0901	-0.117 58	-0.331 68	0.0463
C ₇	0.215 01	0.324 92	0.0076	0.493 08	0.082 44	0.0774	-0.004 38	0.229 57	0.0589

Following an approach already in the literature¹⁴ concerning the use of Ce³⁺ to favor the addition of amines to 6 position of quinolin-5,8-dione, metal(II) acetates (Zn, Cu, and Co) in acetic acid were used to synthesize **5**. Under these conditions, 2-aminophenol (1 mmol) added to a mixture of quinolin-5,8-dione (1 mmol) and Zn(II) acetate (1 mmol) in acetic acid was refluxed for 2 h. **5** was obtained as the main product together with only a trace of **7**. Zn(II) and Co(II) acetates furnished the best results, increasing the **5** yield to 20–30%.

The formation of the quinonimime system of pyridophenoxazinones **5** and **7** seems to be contrary to the results described in the literature by Pratt,¹⁴ who reported that the amines attack the 6 and 7 positions of quinolin-5,8-dione, that the regioselectivity depends on the 6 and 7 charge density, that acid medium and Ce³⁺ ions increase 6-aminoderivative formation, and that no ketimine is recovered.

Pratt's reaction, reexamined by us, yielded the same results when Zn(II) acetate was used instead of Ce³⁺.

Actually, Table 1 shows that the charge density of C₆ is higher than the charge density of C₇ in neutral and acidic media, but the C₇ density charge is higher than C₆ in the Zn(II) quinone complex.

Taking into account our evidence and Pratt's results, a common interpretation can be proposed positing an orbital interaction between the quinonic system of the quinolin-5,8-dione and the soft amino groups of both simple amines and 2-aminophenols according to the frontier orbital theory.¹⁵ This point of view can better explain the different yields of **5** and **7** and the regioselectivity in the 6 and 7 positions in the acid medium in the presence and in the absence of coordinating metal ions.

Table 1 reports, together with the above-mentioned charge density, the HOMO and LUMO coefficients of N-protonated and Zn(II)-complexed quinolin-5,8-dione. In the N-protonated form, present in acetic acid, and more so in the Zn(II)-complexed form, the LUMO coefficients decrease (absolute value) according to 8 > 6 > 7 ≥ 5. Therefore, in acid medium, the nucleophilic attack of an amino group is expected mainly at the carbonyl group in the 8 position and secondarily at the 6 position of the quinolin-5,8-dione.

Nevertheless, the attack of an amine on a carbonyl group is a reversible reaction, and the imine formation is not detectable when it competes with the irreversible

Michael-type reaction. Accordingly, the simple amine addition to quinolin-5,8-dione does not yield ketimines but furnishes only the derivatives at the 6 and 7 positions depending on the orbital coefficients.

In contrast, in the formation of the compound **7**, the attack of the hydroxyl group of the 2-aminophenol on the α,β -unsaturated system shifts the initial unstable 8-hemiaminal toward the formation of the pyridophenoxazinone (Scheme 2). The small yield of compound **5** (compared to **7**) detected in acetic acid can be dependent on the attack of the amino group of 2-aminophenol on the 6 position (having the second largest LUMO coefficient, Table 1). This intermediate furnishes **5** via a multistep reaction involving two molecules of 2-aminophenol named X and Y, respectively (Scheme 3).

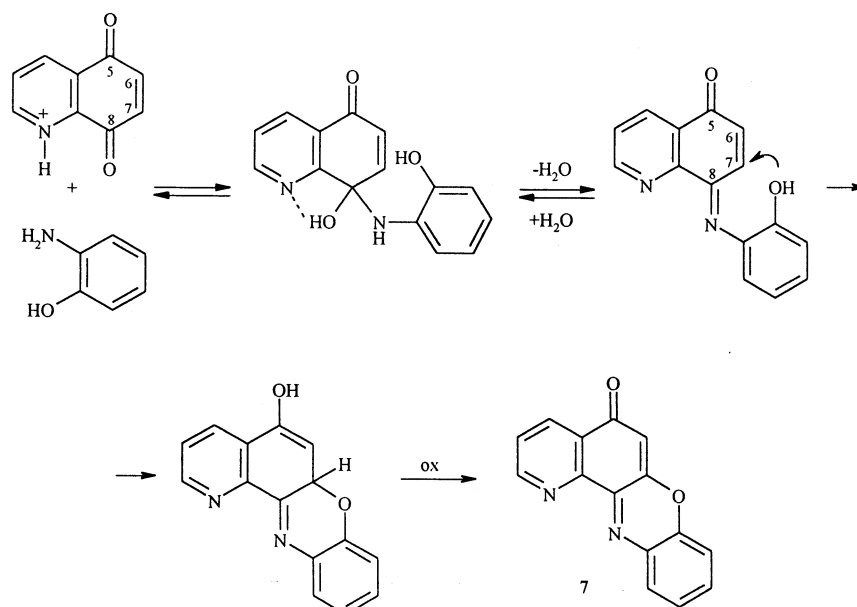
The reaction starts with the attack of the amino group of X on the quinolin-5,8-dione at the 6 position. Quinone reduction takes place and is followed by reoxidation by oxygen or by the quinone present in situ. Subsequently, an intramolecular attack of the hydroxyl group of X to the carbonyl carbon in the 5 position yields a hemiketal, which undergoes a substitution reaction by the amino group of Y, yielding **5** after rearrangement.

The presence of metal(II) acetates under our conditions and of cerious ions under Pratt's conditions,¹⁴ which gives rise to metal quinolin-5,8-dione complex formation, makes the 8 carbonyl carbon unavailable for the nucleophilic attack by steric hindrance and pushes the reaction exclusively at the 6 position.

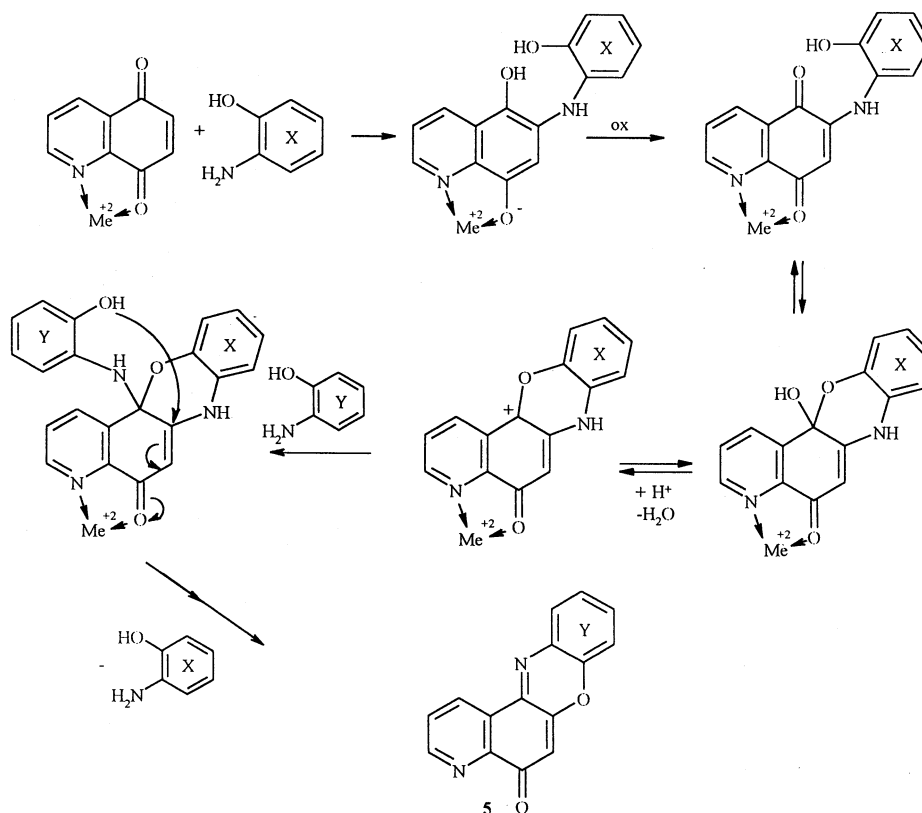
Supporting evidence for the hypothesized formation of **7** (Scheme 2) was obtained by an NMR experiment carried out in the probe of a Bruker 500 MHz spectrometer at 25 °C and in acetic acid-*d*₄. The ¹H NMR spectra of the mixture containing quinolin-5,8-dione and 2-aminophenol were recorded every 10 min. After half an hour, the spectrum showed the decreasing doublets of the starting quinone at δ 7.02 and 7.12, together with two increasing doublets at δ 7.05 and 7.32 interpreted as the hemiaminal formation. After 24 h, the NMR sample, heated, dried in vacuo, and purified chromatographically, yielded **7**.

Moreover, to validate the formation mechanism of **5** proposed in Scheme 3, a reaction between the Zn(II) quinolin-5,8-dione complex and selected 2-aminophenols was performed under the conditions reported in the Experimental Section. Since the attack of the amine group of a substituted aminophenol depends on the aminic nitrogen electron availability, 2-amino-4-nitro-

Scheme 2



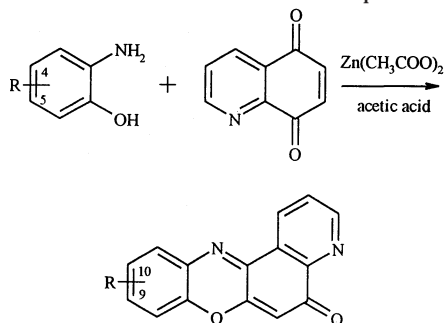
Scheme 3



phenol (**A**) and 2-amino-5-nitrophenol (**B**) were used to prepare 10-nitro- (**8**) and 9-nitropyridophenoxazin-5-one (**9**), respectively. The yield of **8** was larger than the yield of **9** because of the greater reactivity of **A** compared to **B** (Table 2). When the reaction was carried out using equimolar amounts of **A** (1 mmol) and **B** (1 mmol), of Zn(II) acetate (1 mmol), and of quinolin-5,8-dione (1 mmol), pyridophenoxazinones **8** and **9** were recovered from the reaction mixture in nearly equal quantities (Table 2). This result is consistent with the higher reactivity (**A**), which first attacks the 6 position of the metal quinolin-5,8-dione complex. Displacement of **A** by

the less reactive **B**, present at higher concentration and in competition with the unreacted **A**, yields **8** and **9** in the reported ratios (Table 2).

The use of 2-amino-4-methylphenol (**C**) and of 2-amino-5-methylphenol (**D**) yielded the pyridophenoxazinones **10**¹¹ and **11**, respectively. The yields of these reactions (Table 2), **11** > **10** > **8** > **9**, confirmed the dependence of the phenoxazinone formation on electron availability of the amino group of 2-aminophenol, whereas the yields of pyridophenoxazinones, formed in the presence of a mixture of two 2-aminophenol isomers, seem to confirm the displacement reaction proposed in Scheme 3.

Table 2. Reaction between Quinolin-5,8-dione (1 mmol), Zn(II) Acetate (1 mmol), and Substituted 2-Aminophenols (**A**, **B**, **C**, **D**) (1 mmol) in Acetic Acid for 2 h at Reflux Temperature

	substituted 2-aminophenols		yield (%)	ratio
	R	pyridophenoxazinones R		
A	4-NO ₂	8	20	8/9 = 1.66
B	5-NO ₂	9	12	
A + B		8 + 9	15 + 16	8/9 = 0.93
C	4-Me	10	20	
				10/11 = 0.57
D	5-Me	11	35	10/11 = 0.83
C + D		10 + 11	20 + 24	

Table 3. Antitumor Activity of Phenoxazinones **1–5** and Phenothiazinone **6**

compd	IC ₅₀ ^a (μM)				
	CCRF-CEM	CCRF-SB	MT-4	HeLa	Hep-2
1	2.0	1.0	1.2	2.7	1.8
2	0.9	0.5	1.8	2.0	1.5
3	>50.0	3.6	9.5	8.2	1.4
4	19.0	9.0	11.0	13.0	14.2
5	0.01	0.009	0.01	0.2	0.04
6	0.07	0.08	0.08	0.6	0.1
doxorubicin ^b	0.02	0.03	0.01	0.07	0.04
AMD ^b	0.001	0.002	0.001	0.008	0.004

^a Compound concentration required to reduce cell proliferation by 50%, as determined with the MTT method, under conditions allowing untreated controls to undergo at least three consecutive rounds of multiplication. Data represent mean values for three independent determinations. CCRF-CEM, human acute T-lymphoblastic leukemia; CCRF-SB, human acute B-lymphoblastic leukemia; MT-4, human CD4⁺ T cells expressing the TAT gene of HTLV-1; HeLa, cervix carcinoma; Hep-2, larynx carcinoma. ^b Controls.

In conclusion, the study of the formation mechanism of pyridophenoxazinones contributes to clarification of numerous aspects of the general addition of amines to quinones and furnishes a new and effective method for preparing 5*H*-pyrido[3,2-*a*]phenoxazin-5-ones in good amounts by using metal ions.

Antiproliferative Activity. The antiproliferative activity of phenoxazinones **1–4**, pyridophenoxazinone **5**, and pyridophenothiazinone **6** was evaluated against a panel of five human cell lines representative of liquid and solid human tumors, and the results are shown in Table 3. Data for the anticancer agents doxorubicin and AMD are included for comparison. By use of the median of the IC₅₀ values for each compound across the five human cell lines, **5** (median of 0.01 μM) and **6** (median of 0.08 μM) were the most cytotoxic compounds. A profound inhibitory effect was observed on the proliferation of the following human cells, CD4⁺ acute T-lymphoblastic leukemia (CCRF-CEM), acute B-lymphoblastic leukemia (CCRF-SB), CD4⁺ T-cells containing

Table 4. Antitumor Activities of **5** and **6**

cell lines	IC ₅₀ ^a (μM)			
	5	6	doxorubicin ^b	AMD ^b
leukemia/lymphoma				
Wil2-NS	0.05	0.15	0.02	0.0030
Raji	0.04	0.03	0.03	0.0020
MOLT-4	0.04	0.14	0.02	0.0010
C8166	0.10	0.41	0.02	0.0008
MT-4	0.01	0.08	0.01	0.001
carcinoma				
SKMEL-28	0.21	0.81	0.06	0.002
G-361	0.01	0.22	0.09	0.001
MCF-7	0.23	0.65	0.05	0.006
SKMES-1	0.04	0.80	0.03	0.004
HepG-2	0.05	0.11	0.12	0.010
ACHN	0.01	1.92	0.04	0.005
5637	0.01	0.15	0.02	0.003
HT-29	0.25	10.00	0.15	0.006
DU-145	0.04	0.61	0.03	0.008
neuroblastoma				
IMR-32	0.01	0.53	0.01	nd
normal cells				
CRL-7065	0.50	0.81	0.50	0.007

^a Compound concentration required to reduce cell proliferation by 50%, as determined with the MTT method, under conditions allowing untreated controls to undergo at least three consecutive rounds of multiplication. Data represent mean values for three independent determinations. Wil2-NS, human splenic B-lymphoblastoid cells; Raji, human Burkitt lymphoma; MOLT-4, human acute T-lymphoblastic leukemia; C8166 and MT-4, CD4⁺ human acute T-lymphoblastic leukemia; SKMEL-28 and G361, human skin melanoma; MCF-7, human breast adenocarcinoma; SKMES-1, human lung squamous carcinoma; HepG-2, human hepatocellular carcinoma; ACHN, human renal adenocarcinoma; 5637, human bladder carcinoma; HT-29, human colon adenocarcinoma; DU-145, human prostate carcinoma; IMR-32, human neuroblastoma; CRL-7065, human foreskin fibroblasts. ^b Controls.

an integrated HTLV-1 genome (MT-4), cervix carcinoma (HeLa), and larynx carcinoma (Hep-2). The median IC₅₀ value for compounds **2** (median of 1.5 μM) and **3** (median of 8.2 μM) were 150- and 820-fold less than for **5**. The five cell lines were substantially less sensitive to the compounds **1** (median of 1.8 μM) and **4** (median of 13 μM).

Compounds **5** and **6** were evaluated against a larger panel of human lymphoblastoid cell lines, splenic B-lymphoblastoid (Wil2-NS), Burkitt lymphoma (Raji), CD4⁺ acute T-lymphoblastic leukemia (MOLT-4), and CD4⁺ T-cells containing an integrated HTLV-1 genome (C8166). Furthermore, **5** and **6** exhibited significant potency on solid-human-tumor-derived cells, skin melanoma (SKMEL-28 and G361), breast adenocarcinoma (MCF-7), lung squamous carcinoma (SKMES-1), hepatocellular carcinoma (HepG-2), renal adenocarcinoma (ACHN), bladder carcinoma (5637), colon adenocarcinoma (HT-29), prostate carcinoma (DU-145), neuroblastoma (IMR-32), and foreskin fibroblasts (CRL-7065). It is interesting to note that the cell lines of liquid tumors are 2.5-fold more susceptible to the cytotoxic action than the solid-tumor-derived cells. The CCRF-SB, CCRF-CEM, G361, ACHN, and 5637 cell lines were substantially more sensitive to compound **5**, which exhibited cytotoxic activities comparable to or 2- to 3-fold higher than doxorubicin, used as control (Table 4).

As evident from Tables 3 and 4, the IC₅₀ for **5** ranged between 0.05 and 0.009 μM with respect to a larger number of tested cell lines. The same compound showed the maximum of potency against CCRF-SB (IC₅₀ = 0.009 μM). The phenothiazinone **6** demonstrated the

Table 5. Cytotoxicity of **5** for Normal Human Lymphocytes

	CC ₅₀ ^a (μM)		
	PBL _{resting} ^b	PBL _{PHA} ^c	leukemia ^d
5	5.0 (±0.2)	0.03 (±0.003)	0.04
AMD	0.002 (±0.001)	0.005 (±0.001)	0.003
doxorubicin	0.09 (±0.03)	0.04 (±0.005)	0.02

^a Compound concentration required to reduce cell multiplication by 50%. Values are the mean (±SD) for three separate experiments. ^b Peripheral blood lymphocytes (PBL) were treated with test drugs for 3 days, then resuspended in drug-free medium and stimulated with phytohemagglutinin (PHA). ^c PBL were stimulated with PHA and then resuspended in IL2-containing medium in the presence of drugs. ^d Data are the mean IC₅₀ values obtained with lymphoblastoid cell lines.

highest potency against the panel of lymphoblastoid cell lines (median of 0.08 μM), especially against MT-4 and Raji with IC₅₀ values of 0.08 and 0.03 μM, respectively. Against 5637 and Hep-2 cells, **6** also showed potent cytotoxic activity (IC₅₀ = 0.1 μM).

Cytotoxicity for Normal Cells. To evaluate whether pyridophenoxazinone **5**, AMD, and doxorubicin were cytotoxic for normal human cells, resting peripheral blood lymphocytes (PBL) from healthy donors were pretreated for 3 days with various serial dilutions of test compounds and then allowed to proliferate in drug-free medium following stimulation with phytohemagglutinin (PHA). While pretreatment with **5** had no effect on cell proliferation, even when used at concentrations up to 5 μM, AMD and doxorubicin were cytotoxic at the concentrations at which they inhibit leukemia cells (Table 5). **5**, AMD, and doxorubicin inhibited cell proliferation at concentrations (0.03 μM) comparable to those active against leukemic cell lines when they were added to PHA-stimulated PBL. In conclusion, **5** differs from AMD and doxorubicin in being noncytotoxic for resting PBL.

Antiproliferative Activity against Drug-Resistant Tumor Cell Lines. Drug resistance is a relevant therapeutic problem caused by the emergence of tumor cells that confer resistance to a variety of anticancer drugs. The most common mechanisms of drug resistance are related to the overexpression of glycoproteins capable of mediating the efflux of different drugs such as doxorubicin, vincristine, and etoposide and to the altered contents of target enzymes (topoisomerases I and II). Therefore, the inhibitory activity of **5** was evaluated against the following KB subclones (Table 6): (i) KB^{MDR}, obtained by infection of KB^{wt} with a retroviral vector carrying the human *mdr-1* gene and maintained under uninterrupted treatment with doxorubicin, these cells expressing a membrane glycoprotein (Pgp) responsible for the efflux of many unrelated drugs (multidrug resistance or MDR);^{16,17} (ii) KB^{V20C}, selected under

uninterrupted treatment with vincristine, these cells possessing an MDR phenotype^{18,19} related to the overexpression of the *mdr-1* gene and mediating the efflux of doxorubicin, vincristine, and etoposide; (iii) KB^{7D}, selected under uninterrupted treatment with etoposide, a topoisomerase II inhibitor for clinical use.²⁰ The resistance is due to overexpression of the *mrp* gene, which codes for a membrane glycoprotein (MRP) capable of mediating the efflux of etoposide, doxorubicin, and vincristine. These cells also express altered levels of topoisomerase II. Interestingly, **5** proved to be fully inhibitory to all these resistant cell lines, thus suggesting that it is not subject to the pump mediating the efflux of many antitumor drugs and that it does not interfere with DNA synthesis by affecting the topoisomerase II catalyzed step.

Structure–Activity Relationships. The antitumor activity in vitro, in the increasing order **4** < **3** < **1** < **2** < **6** < **5**, seems to be correlated with the presence of either a protonable nitrogen at position 2 of the phenoxazinone system or a π-density on the α-carbon at position 1 (**2**, **5**, **6**). The absence of the amino function in the 2 position (**4**) and its transformation in an *N*-acetyl group (**3**) are detrimental for activity.

Although the phenoxazinone system has been considered determining for the AMD intercalation into DNA strands, the median IC₅₀ for **4** shows that the simple phenoxazinone nucleus is incapable of inhibiting the cellular proliferation at low concentrations (median of 13 μM). Consequently, it is reasonable to suppose that this planar scaffold requires hydrogen bonding acceptor/donor groups and additional π-sites, like double-bonded substituents or fused rings, to promote stacking interactions. The diacetyl groups mimicking the peptide chains of AMD appear to make **2** (median of 1.5 μM) slightly more active than **1** (median of 1.8 μM), suggesting that the analogy between acetyl groups and peptide chains is not the discriminating factor for activity, which rather depends on the presence of the π-site of carbonyl. In fact, **2** is 150- and 20-fold less active compared to the highly conjugated tetracyclic compounds **5** (median of 0.01 μM) and **6** (median of 0.08 μM).

When compared to **1** (median of 1.8 μM), the poor activity of the *N*-acetyl derivative **3** (median of 8.2 μM) could be ascribed to the low tendency of the amidic nitrogen to act as a lone pair donor and/or the steric hindrance of the acetyl group and/or the formation of an intramolecular hydrogen bond between the enolic hydrogen and the quinonic oxygen. Compound **6**, isosteric with **5**, containing a larger and lipophilic endocyclic sulfur atom, showed a slightly decreased antiproliferative activity (median of 0.08 μM).

Table 6. Effect of **5** on the Proliferation of Wild-Type and Drug-Resistant KB Cells

compd	IC ₅₀ ^a (μM)			
	KB _{WT} ^b	KB ^{MDR} ^c	KB ^{7D} ^d	KB ^{V20C} ^e
5	0.1 (±0.1)	0.04 (±0.02)	0.02 (±0.01)	0.06 (±0.02)
doxorubicin	0.06 (±0.02)	1.8 (±0.1)	2.8 (±0.2)	0.4 (±0.1)
AMD	0.005 (±0.001)	0.2 (±0.1)	0.2 (±0.1)	0.05 (±0.01)
vincristine	0.006 (±0.001)	0.7 (±0.2)	0.05 (±0.01)	0.2 (±0.1)
etoposide	0.6 (±0.1)	>20	>20	6.2 (±1.2)

^a Compound concentration required to reduce cell proliferation by 50%, as determined with the MTT method, under condition allowing untreated controls to undergo at least three consecutive rounds of multiplication. Data represent mean values (±SD) for three independent determinations. ^b KB human nasopharyngeal carcinoma. ^c KB subclones passaged in the presence of doxorubicin 0.09 μM. ^d KB subclones passaged in the presence of etoposide 7 μM. ^e KB subclones passaged in the presence of vincristine 0.02 μM.

On the basis of the experimental evidence, three possible reasons can be proposed to justify the importance of the fused pyridine ring on the phenoxazinone system of **5**, which exhibits an activity value much higher than the corresponding parent molecule **1** (median of 1.8 μM): (i) the formation of a hydrogen bond between the pyridine nitrogen and an acceptor site of the DNA strand; (ii) the strength and the extent of stacking forces between superposed and parallel aromatic fused rings; (iii) the size of the tetracyclic system giving a better fit into the intercalation binding site.

DNA-Binding Properties. Compound **5** was tested to see if it interacts with DNA, using spectrophotometric measurements and a preliminary ^1H NMR investigation. The spectroscopic properties of **5** in the presence and absence of calf thymus DNA were studied by conventional optical spectroscopy. Characterization of this mixture was done by comparing the UV–vis absorption spectrum of the complex with the spectrum of the sample in a phosphate buffer at pH 7. The DNA-bound **5** showed hypochromism (30% reduction in extinction coefficient) and a red shift in the absorption band (absorption maximum from 442 to 447 nm and two isosbestic points at 320 and 515 nm). These spectral changes suggest that this compound presents a single binding with DNA.

A titration of the $[\text{d}(\text{GAAGCTTC})]_2$ octamer expressly synthesized was carried out in the probe of a Bruker AMX 500 MHz spectrometer at 10 °C by addition of small aliquots of **5** until a 1:1 ratio of **5**/octamer was reached. The ^1H NMR spectra were recorded in 5 min time intervals between the additions of **5** to allow binding equilibration. A comparison of the chemical shifts of the aromatic protons of **5** and $[\text{d}(\text{GAAGCTTC})]_2$ with those of the $5/[\text{d}(\text{GAAGCTTC})]_2$ complex showed that all resonances shift toward higher fields upon drug addition (Figure 1). All the chemical shifts of **5** in the complex are shielded compared to those of the free drug, with the protons H1, H8, and H11 exhibiting shields of 0.60, 0.41, and 0.45 ppm, respectively. The most significant shifts of the octamer are due to the H8 proton of the guanine G4 (from δ 7.65 to 7.55) and to protons H6 and H5 of cytosine C5 (from δ 7.36 to 7.31 and from δ 5.77 to 5.74, respectively). Table 7 reports the proton chemical shift assignments of **5**, of G4 and of C5 in the $5/[\text{d}(\text{GAAGCTTC})]_2$ complex, and their comparison with unbounded ligand and free octamer. These results provide further evidence that **5** binds to DNA and that intercalation occurs altering the base sequence GC.

Model Building and MD Simulation of the $5/[\text{d}(\text{GAAGCTTC})]_2$ Complex. On the basis of the X-ray crystal structure of N8-AMD bound to $[\text{d}(\text{GAAGCTTC})]_2$ ⁸ and of the ^1H NMR study on the binding of **5** to $[\text{d}(\text{GAAGCTTC})]_2$, a model of the octamer complexed to compound **5** was built by manual docking and extensive energy minimization and equilibration, as described in the Experimental Section.

The pyridine nitrogen of the ligand was taken as protonated, as suggested from the pK_a of its conjugated acid (5.9). This value is quite low compared to physiological pH so that only a small fraction of the agent will be protonated. However, it is well-known^{21,22} that the pK_a of intercalators of this type rises about 1–1.5 pK units when intercalated into DNA. So, we may

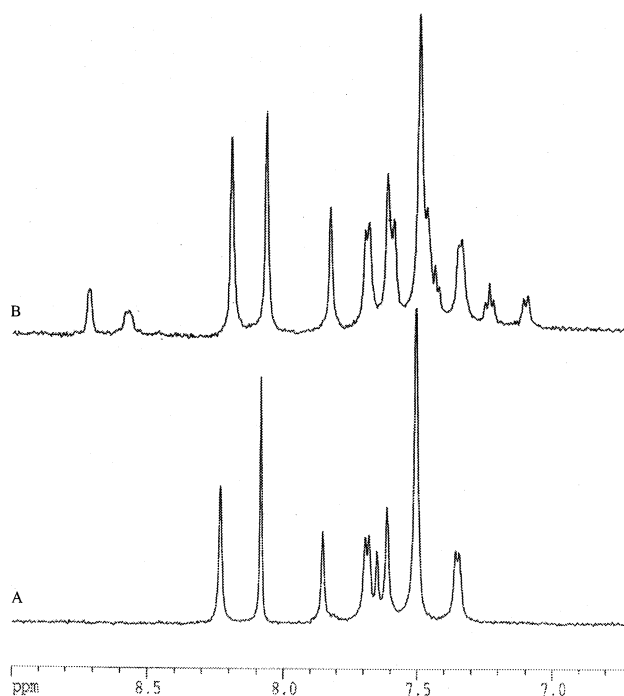


Figure 1. ^1H NMR chemical shift variations of the aromatic region of (A) free octamer $[\text{d}(\text{GAAGCTTC})]_2$ and (B) 1:1 $5/[\text{d}(\text{GAAGCTTC})]_2$ complex were recorded at 10 °C on a 500 MHz spectrometer.

Table 7. Proton Chemical Shift Assignments of Unbounded **5** and of Guanine G4 and Cytosine C5 in the Free Octamer $[\text{d}(\text{GAAGCTTC})]_2$ and Their Comparison with the $5/[\text{d}(\text{GAAGCTTC})]_2$ Complex

	unbounded 5 , δ	$5/[\text{d}(\text{GAAGCTTC})]_2$, δ	$\Delta\delta$
H-1	8.96	8.56	-0.60
H-2	7.88	7.58	-0.30
H-3	9.02	8.71	-0.31
H-6	6.54	6.25	-0.29
H-8	7.51	7.10	-0.41
H-9	7.63	7.42	-0.21
H-10	7.41	7.22	-0.19
H-11	7.88	7.43	-0.45
guanine G4 in			
	$[\text{d}(\text{GAAGCTTC})]_2$, δ	$5/[\text{d}(\text{GAAGCTTC})]_2$, δ	$\Delta\delta$
H-8	7.65	7.55	-0.10
cytosine C5 in			
	$[\text{d}(\text{GAAGCTTC})]_2$, δ	$5/[\text{d}(\text{GAAGCTTC})]_2$, δ	$\Delta\delta$
H-5	5.52	5.53	+0.01
H-6	7.36	7.31	-0.05

expect that the pK_a of bound **5** is probably about 7–7.5, which explains why it binds so well at pH 7 and why it is biologically active.

The pyridophenoxazinone chromophore binds at the middle 5'-GC-3' base pairs of double-stranded DNA by intercalation (Figure 2).

A free MD trajectory (70 ps) was generated at 300 K for a fully solvated complex using PME to calculate electrostatic forces. The trajectory was sampled every 1 ps and examined visually by using the SYBYL program.²³ Inspection of the MD trajectory, during which the drug remains inserted in the DNA and fully intercalating at the 5'-GC-3' steps, leads to the following observations: Watson–Crick base–base hydrogen bond distances are conserved during the simulation with an

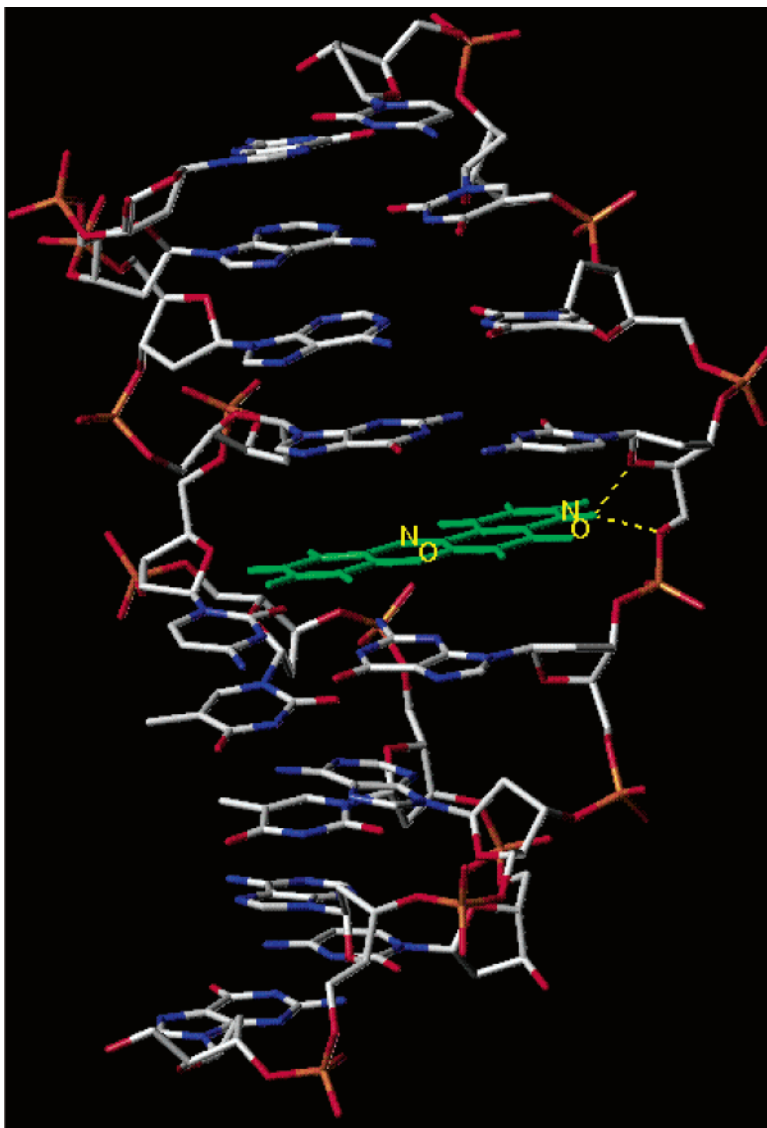


Figure 2. Side view of the energy-minimized average structure from the 70 ps period of the MD simulation in water of [d(GAAGCTTC)]₂ complexed to pyridophenoxazinone **5**.

average value around 2 Å; average Watson–Crick base–base distance C1′–C1′ and base–base angle N1–C1′–C1′ for pyrimidines or N9–C1′–C1′ for purines are 10.7 Å and 65.4° with root-mean-square deviations (rmsd) of 0.2 Å and 8°, respectively, in agreement with standard values for B-DNA (10.85 Å and 51.5°).²⁴

The plot of the total (solid line) and potential energies (dotted line) over the final 70 ps of the simulation confirms that the system is energetically stable during the production run (Figure 3A). This is consistent with the temperature and pressure trajectory of the system, which also remain virtually constant throughout the MD production runs. A rough measure of the conformational changes undergone by the complex is provided by continuous monitoring of the rmsd from the initial structure. The average rmsd calculated for all atoms from the initial energy-minimized complex is shown in Figure 3B. After the initial heating to 300 K, the rmsd profile remains stable for the rest of the simulation (1.6 ± 0.3 Å), indicating that the drug/DNA complex settles into a well-defined and stable configuration during the simulation. The average distance between the **5** and the DNA centers of mass was also monitored during the

trajectory. The deviation in this value is quite small and suggests that **5** is docked to the DNA in a stable local minimum (Figure 3C). This shows the occurrence of good π – π interactions between the pyridophenoxazinone nucleus and the base pairs at the binding site. The distance separating the ligand and DNA centers of mass is significantly small (1.9 ± 0.5 Å).

As shown in Figures 2 and 4, the complex **5**/[d(GAAGCTTC)]₂ is stabilized by hydrogen bonds and by π – π stacking forces. The hydrogen of the positively charged pyridine nitrogen of **5** forms a hydrogen bond with O4′ in the deoxyribose ring of the cytosine C5 residue at the intercalation site. The protonated nitrogen also participates in a hydrogen bond with O5′ of the phosphate backbone located between the G4 and C5 residues. These hydrogen-bonding interactions were present in the initial model and were maintained for the whole length of the monitored simulation period. The protonated nitrogen of **5** is also close to the oxygen O1 of the phosphate group of cytosine C5 so that an additional favorable electrostatic interaction might be established when **5** binds to the DNA. In our MD simulations, this last hydrogen bond, initially present

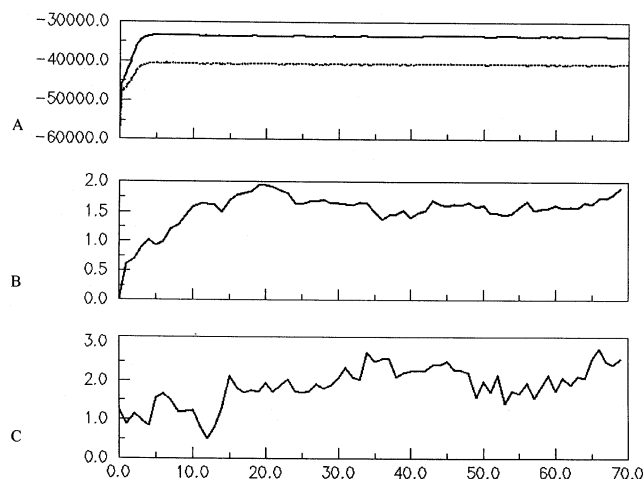


Figure 3. Plots of the trajectory of the intercalation model: (A) time dependence of total (solid line) and potential (dotted line) energies in kcal/mol during the simulation; (B) time dependence of rmsd of atomic coordinates for the 5/[d(GAAGCTTC)]₂ complex relative to the energy-minimized starting structure for 70 ps of unrestrained MD, in Å; (C) time dependence of distances between pyridophenoxazinone **5** and DNA centers of mass for the 5/[d(GAAGCTTC)]₂ complex, in Å.

in the complex, was maintained during the first 20 ps of simulation and gradually lost during the next 50 ps sampling period, probably owing to competition with solvent molecules.

The model reported in Figure 4 suggests that the intercalation of **5** with DNA also involves π - π stacking interactions of the rings A, B, C, and D: (i) A and B interact with the five- and six-membered rings of the overlying guanine G12; (ii) B and C interact with the six- and five-membered ring of the underlying guanine G4; (iii) iminoquinone C interacts with the six-membered ring of the overlying cytosine C5; (iv) pyridine D interacts with the six-membered ring of guanine G4. Such interactions, which give rise to slipped face-centered geometries, are consistent with SAR data of these compounds and justify the higher activity of tetracyclic **5** and **6**. These findings are in accordance with the pharmacophoric role that we assigned to the pyridine nitrogen prompted by SAR data.

Conclusions

In this paper we have described a series of polycyclic iminoquinonic compounds, phenoxazinones **1**–**4**, pyri-

dophenoxazinone **5**, and pyridophenothiazinone **6**, which exhibit activity against leukemia and solid tumor cell lines at submicromolar concentrations. The most active pyridophenoxazinone **5**, unlike doxorubicin, showed a low cytotoxicity for PBL_{resting} normal cells. Moreover, **5** exhibited fully inhibitory activity against MDR cells, thus suggesting that it neither is subject to the pump mediating the efflux of many antitumor drugs nor interferes with the DNA synthesis by affecting the topoisomerase II catalyzed step. In summary of the SAR data, optimum antiproliferative inhibition was obtained with tetracyclic compounds **5** containing a pyridine[3,2-*a*] fused with the phenoxazinone nucleus and its phenothiazinone isosteric **6**. The pyridine nitrogen of **5** and **6** lies in the corresponding position of the 2-amino group of AMD. Additional π -sites in position 1 are critical for activity, enhancing the stacking forces.

A red shift and a hypochromic effect were recorded by UV-vis measurements of the 5/[d(GAAGCTTC)]₂ complex. To validate the hypothesis of a common DNA intercalation binding site between the AMD chromophore and **5**, a ¹H NMR investigation was performed on the 5/[d(GAAGCTTC)]₂ complex and a three-dimensional structural model was developed. Compound **5**, which intercalates at the middle 5'-GC-3' base pairs of double-stranded DNA, is stabilized by π - π stacking interactions and by a proposed set of hydrogen bonds. The ligand probably approaches DNA with the positively charged pyridine nitrogen pointed toward the minor groove of DNA. This charged group might interact with the negatively charged oxygen atoms (O4' and O5') of the cytosine C5 residue in the minor groove, making the insertion of the pyridophenoxazinone between the base pairs easier. This proposed intercalation process could explain the high cytotoxicity of this series of compounds. An original procedure for the synthesis of 5*H*-pyrido[3,2-*a*]phenoxazin-5-one (**5**), by metal assistance, is reported, and the reaction between quinolin-5,8-dione and 2-aminophenols has been investigated.

Experimental Section

Chemistry. Melting points were determined with a Kofler apparatus and are uncorrected. The elemental analysis results (C, H, and N) of reported compounds agree with the calculated values and were within $\pm 0.4\%$ of theoretical values. Electron impact (EI) mass spectra were obtained at 70 eV on a ZAB 2F spectrometer. The purity of compounds was checked by ascending TLC on Merck's silica gel plates (0.25 mm) with

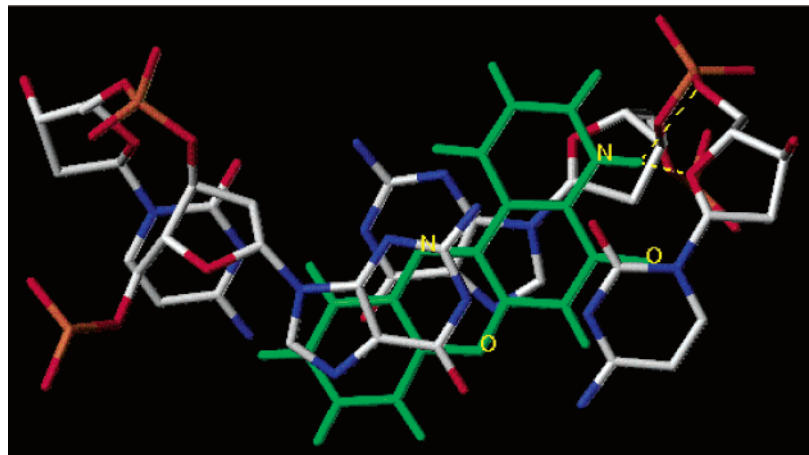


Figure 4. Intercalation site of the 5/[d(GAAGCTTC)]₂ complex viewed in a projection plane orthogonal to the helix axis.

fluorescent baking. The UV spectra were recorded on a Perkin-Elmer 550S spectrometer. The IR spectra were taken on a Perkin-Elmer 399 spectrometer in KBr. The C=O and C=N stretches lie between 1628 and 1635 cm^{-1} . ^1H NMR spectra (data reported in δ) were recorded on a Bruker AMX 500 MHz spectrometer with Me_4Si as internal reference.

2-Amino-3H-phenoxazin-3-one (1). Mp, 256–6 °C. UV (CHCl_3) λ_{max} , nm (log ϵ): 421–36 (4.10). ^1H NMR (CDCl_3): δ 7.76 (1H, d, $J = 8.1$ Hz), 7.38 (1H, d, $J = 8.0$ Hz), 7.40 (1H, t, $J = 8.0$ Hz), 7.42 (1H, t, $J = 8.1$ Hz), 6.52 (1H, s), 6.44 (1H, s), 5.16 (NH_2 , bs, D_2O exchangeable). MS m/z : 212 (M^+). Anal. ($\text{C}_{12}\text{H}_8\text{N}_2\text{O}_2$) C, H, N.

2-Amino-1,9-diacetyl-3H-phenoxazin-3-one (2). Mp, 290–1 °C. UV (CHCl_3) λ_{max} , nm (log ϵ): 430 (4.42), 410 (4.35), 330 (3.71). ^1H NMR (CDCl_3): 7.46 (1H, d, $J = 7.9$ Hz), 7.45 (1H, t, $J = 7.9$ Hz), 7.42 (1H, d, $J = 7.9$ Hz), 7.12 (2H, bs, D_2O exchangeable), 6.51 (1H, s), 2.79 (3H, s), 2.73 (3H, s). MS m/z : 296 (M^+). Anal. ($\text{C}_{16}\text{H}_{12}\text{N}_2\text{O}_4$) C, H, N.

2-Acetyl-amino-3H-phenoxazin-3-one (3). Mp, 165–6 °C. UV (CHCl_3) λ_{max} , nm (log ϵ): 403 (4.24). ^1H NMR (CDCl_3): 8.55 (1H, bs, D_2O exchangeable), 8.44 (1H, s), 7.88 (1H, d, $J = 7.9$ Hz), 7.55 (1H, t, $J = 7.9$ Hz), 7.41 (1H, t, $J = 7.9$ Hz), 7.41 (1H, d, $J = 7.9$ Hz), 6.47 (1H, s), 2.13 (3H, s). MS m/z : 254 (M^+). Anal. ($\text{C}_{14}\text{H}_{10}\text{N}_2\text{O}_3$) C, H, N.

3H-Phenoxazin-3-one (4). Mp, 205–6 °C. UV (CHCl_3) λ_{max} , nm (log ϵ): 449 (3.95); 348 (3.9). ^1H NMR (CDCl_3): 7.87 (1H, d, $J = 7.8$ Hz), 7.60 (1H, t, $J = 7.8$ Hz), 7.50 (1H, d, $J = 8.0$ Hz), 7.38 (1H, t, $J = 7.7$ Hz), 7.35 (1H, d, $J = 7.7$ Hz), 6.87 (1H, d, $J = 8.0$), 6.25 (1H; s). MS m/z : 197 (M^+). Anal. ($\text{C}_{12}\text{H}_7\text{N}_2\text{O}$) C, H, N.

5H-Pyrido[3,2-a]phenothiazin-5-one (6). Mp 228–9 °C. UV (CHCl_3) λ_{max} , nm (log ϵ): 452 (3.5). ^1H NMR (CDCl_3): 9.18 (1H, d, $J = 4.5$ Hz), 9.08 (1H, d, $J = 8.0$ Hz), 7.96 (1H, d, $J = 7.9$ Hz), 7.71 (1H, dd, $J = 4.5, 8.0$ Hz), 7.53 (1H, t, $J = 8.0$ Hz), 7.49 (1H, t, $J = 8.0$ Hz), 7.45 (1H, d, $J = 8.0$ Hz), 7.01 (1H, s). MS-EI m/z : 264 (M^+), 266 ($\text{M} + 2, 11\% \text{M}^+$), 268 ($\text{M} + 4, 4\% \text{M}^+$). Anal. ($\text{C}_{15}\text{H}_8\text{N}_2\text{OS}$) C, H, N.

5H-Pyrido[2,3-a]phenoxazin-5-one (7). Mp 235 °C. UV (CHCl_3) λ_{max} , nm (log ϵ): 435 (4.09). ^1H NMR (CDCl_3): 9.15 (1H, d, $J = 4.0$ Hz), 8.63 (1H, d, $J = 8.1$ Hz), 8.11 (1H, d, $J = 8.1$ Hz), 7.72 (1H, dd, $J = 4.0, 8.1$ Hz), 7.56 (1H, t, $J = 8.1$ Hz), 7.41 (1H, t, $J = 8.0$ Hz), 7.35 (1H, d, $J = 8.0$ Hz), 6.51 (1H, s). MS-EI m/z : 248 (M^+). Anal. ($\text{C}_{15}\text{H}_8\text{N}_2\text{O}_2$) C, H, N.

Substituted 5H-pyrido[3,2-a]phenoxazin-5-ones. General Procedure. Substituted 2-aminophenols (0.01 mol) in methanol-acetic acid (50:50; v/v, 10 mL) were added dropwise to an equimolar mixture of quinolin-5,8-dione (0.01 mol) and Zn(II) acetate (0.01 mol) in acetic acid (50 mL) stirred and gently warmed until the dark color showed the complex formation. The reaction mixture refluxed for 2 h was evaporated in vacuo, diluted by water, acidified (HCl 6N) to break the Zn(II)-complex and extracted (CHCl_3). The organic layer, evaporated in vacuo and purified on silica gel column (CHCl_3 : CH_3OH 9.5:0.5 v:v as eluent) afforded the pyridophenoxazinones **5**, **8**, **9**, **10** and **11**, which were crystallized from ethyl acetate.

5H-Pyrido[3,2-a]phenoxazin-5-one (5). Mp 246–7 °C. UV (CHCl_3) λ_{max} , nm (log ϵ): 429 (3.87); 348 (3.86). ^1H NMR (CDCl_3): 9.08 (1H, d, $J = 4.0$ Hz), 9.05 (1H, d, $J = 8.1$ Hz), 7.83 (1H, d, $J = 8.2$ Hz), 7.72 (1H, dd, $J = 4.0, 8.1$ Hz), 7.55 (1H, t, $J = 8.1$ Hz), 7.38 (1H, t, $J = 8.1$ Hz), 7.35 (1H, d, $J = 8.2$ Hz), 6.63 (1H, s). MS-EI m/z : 248 (M^+). Anal. ($\text{C}_{15}\text{H}_8\text{N}_2\text{O}_2$) C, H, N.

10-Nitro-5H-pyrido[3,2-a]phenoxazin-5-one (8). Mp 295–6 °C. UV (CHCl_3) λ_{max} , nm (log ϵ): 413 (3.82). ^1H NMR (CDCl_3): 9.15 (1H, d, $J = 4.0$ Hz), 9.06 (1H, d, $J = 8.1$ Hz), 8.74 (1H, s), 8.41 (1H, d, $J = 8.6$ Hz), 7.79 (1H, dd, $J = 4.0, 8.1$ Hz), 7.48 (1H, d, $J = 8.6$ Hz), 6.71 (1H, s). MS-EI m/z : 293 (M^+). Anal. ($\text{C}_{15}\text{H}_7\text{N}_3\text{O}_4$) C, H, N.

9-Nitro-5H-pyrido[3,2-a]phenoxazin-5-one (9). Mp 314–5 °C. UV (CHCl_3) λ_{max} , nm (log ϵ): 441 (3.17), 430 (3.16). ^1H NMR (CDCl_3): 9.15 (1H, d, $J = 4.0$ Hz), 9.06 (1H, d, $J = 8.4$ Hz), 8.24 (1H, d, $J = 8.7$ Hz), 8.22 (1H, s), 8.01 (1H, d, $J = 8.7$ Hz),

7.79 (1H, dd, $J = 4.0, 8.4$ Hz), 6.71 (1H, s). MS-EI m/z : 293 (M^+). Anal. ($\text{C}_{15}\text{H}_7\text{N}_3\text{O}_4$) C, H, N.

10-Methyl-5H-pyrido[3,2-a]phenoxazin-5-one (10). Mp 201–2 °C. UV (CHCl_3) λ_{max} , nm (log ϵ): 433 (3.72). ^1H NMR (CDCl_3): 9.08 (1H, d, $J = 4.1$ Hz), 9.04 (1H, d, $J = 8.0$ Hz), 7.70 (1H, dd, $J = 4.1, 8.0$ Hz), 7.67 (1H, s), 7.34 (1H, d, $J = 7.8$ Hz), 7.25 (1H, d, $J = 7.8$ Hz), 6.62 (1H, s), 2.47 (3H, s). MS-EI m/z : 262 (M^+). Anal. ($\text{C}_{16}\text{H}_{10}\text{N}_2\text{O}_2$) C, H, N.

9-Methyl-5H-pyrido[3,2-a]phenoxazin-5-one (11). Mp 232–3 °C. UV (CHCl_3) λ_{max} , nm (log ϵ): 434 (3.72). ^1H NMR (CDCl_3): 9.00 (1H, d, $J = 4.2$ Hz), 8.94 (1H, d, $J = 7.9$ Hz), 7.65 (1H, d, $J = 7.9$ Hz), 7.63 (1H, d, $J = 7.7$ Hz), 7.13 (1H, d, $J = 7.7$ Hz), 7.06 (1H, s), 6.51 (1H, s), 2.43 (3H, s). MS-EI m/z : 262 (M^+). Anal. ($\text{C}_{16}\text{H}_{10}\text{N}_2\text{O}_2$) C, H, N.

Reaction between Quinolin-5,8-dione and a Mixture of Two Isomeric Substituted 2-Aminophenols. General Procedure. A mixture of 2-amino-4-substituted phenol (1 mmol) and 2-amino-5-substituted phenol (1 mmol) in acetic acid (10 mL) was added dropwise to a mixture of quinolin-5,8-dione (1 mmol) and Zn(II) acetate (1 mmol) in acetic acid (20 mL), stirred, and gently warmed until the dark color indicated complex formation. The reaction mixture was refluxed for 2 h, evaporated in vacuo, diluted by water, acidified (6 N HCl) to break the Zn complex, and extracted (CHCl_3). The organic layer, evaporated in vacuo and purified on a silica gel column (CHCl_3 : CH_3OH 9.5:0.5 v/v, as eluent) afforded the corresponding couples of pyridophenoxazinones **8/9** and **10/11**, respectively.

Ab Initio Calculations. All the computations were performed with a modified version of the Gaussian 98 package.²⁵ The geometries of quinonoid compounds have been fully optimized by the PBE0²⁶ density functional using the 6-31G^{27,28} basis set.²⁹ The reliability of this procedure is documented in a number of recent studies.^{26,28,29} Atomic charges have been obtained at the same level using a Mülliken population analysis, whereas HOMO and LUMO coefficients have been computed at the HF/STO-3G level using the same geometries.

Biology. Compounds. Test compounds were dissolved in DMSO at an initial concentration of 200 μM and then were serially diluted in culture medium.

Cells. Cell lines were from American Type Culture Collection (ATCC). The human nasopharyngeal carcinoma KB cell line and the drug-resistant subclones KB^{MDR}, KB^{V20C}, and KB⁷⁰ were a generous gift from Prof. Y. C. Cheng, Yale University. Liquid-tumor-derived cell lines were grown in RPMI 1640 containing 10% fetal calf serum (FCS), 100 U/mL penicillin G, and 100 $\mu\text{g}/\text{mL}$ streptomycin. Solid-tumor-derived cells were grown in their specific media supplemented with 10% FCS and antibiotics. Cell cultures were incubated at 37 °C in a humidified 5% CO_2 atmosphere. Cell cultures were checked periodically for the absence of mycoplasma contamination by the Hoechst staining method.

Antiproliferative Assays. Exponentially growing leukemia and lymphoma cells were resuspended at a density of 1×10^5 cells/mL in RPMI containing serial dilutions of the test drugs. Cell viability was determined after 96 h at 37 °C by the 3-(4,5-dimethylthiazol-2-yl)-2,5-diphenyltetrazolium bromide (MTT) method. Activity against solid-tumor-derived cells was evaluated in exponentially growing cultures seeded at 5×10^4 cells/mL and allowed to adhere for 16 h to culture plates before addition of the drugs. Cell viability was determined by the MTT method 4 days later.

Linear Regression Analysis. Tumor cell growth at each drug concentration was expressed as a percentage of untreated controls, and the concentration resulting in 50% (CC_{50} , IC_{50}) growth inhibition was determined by linear regression analysis.

Cytotoxicity Assays. Peripheral blood lymphocytes (PBL) from HIV-negative donors were obtained by separation on Fycoll–Hypaque gradients. After extensive washings, cells were resuspended (1×10^6 cells/mL) in RPMI-1640 with 10% FCS and incubated overnight. For cytotoxicity evaluations in proliferating PBL cultures, nonadherent cells were resuspended at 1×10^6 cells/mL in growth medium, stimulated with

PHA (2.5 $\mu\text{g/mL}$) for 24 h before dilution to 1×10^5 cells/mL in medium containing PHA (2.5 $\mu\text{g/mL}$), IL-2 (50 U/mL), and various concentrations of the test compounds. Viable cell number was determined 6 days later. Under these conditions, untreated PBL were able to undergo exponential growth up to four cell cycles, as determined by viable cell counts. For cytotoxicity evaluations in resting PBL cultures, nonadherent cells were resuspended at high density (1×10^6 cells/mL) and treated for as long as 3 days with the test compounds. Then, the cells were extensively washed to remove the inhibitors and were stimulated with PHA for 24 h before being diluted to 1×10^5 cells/mL in medium containing PHA and IL-2. Cell viability was determined after incubation at 37 °C for 6 days.

pK_a Determination of 5. A solution in Nanopure water of a hydrochloride salt, or free base of **5** (0.008 mM), NaCl (3.2 mM), and EDTA (0.08 mM) in a 1 cm UV cell was titrated with either NaOH (0.01 mM) or HCl (0.01 mM). After each addition of the base or the acid, the pH was measured on an Avantech Crison Mod GLP21 pH meter using a microprobe glass electrode with an Ag/HCl reference, and the UV-vis spectrum (250–600 nm) was taken on a Perkin-Elmer 550S UV-vis spectrophotometer. The total increase in volume at the end of titration did not exceed 1%. For each compound, the absorption spectra were determined in a range of pH values at least 2 orders of magnitude from the pK_a value, and at least two measurements per pH unit were made. The spectral shifts with excellent isosbestic points in the spectra were obtained. The absorption data for each measurement were overlaid, and the absorption of the wavelength of greatest change in the spectra was extracted, normalized, and plotted as a function of pH. The pK_a value for the protonated N4 atom of pyridophenoxazinone **5** was calculated from the midpoint of changes in optical behavior.

Spectrophotometry. Molar extinction coefficients at the wavelength of maximum absorption in the visible spectrum were determined for **5** free in solution, bound to calf thymus DNA (Sigma Chemical Company, St. Louis, MO) using a Perkin-Elmer 550S UV-vis spectrophotometer.

Measurements were made in 0.1 M SHE buffer [2 mM 4-(2-hydroxyethyl)-1-piperazineethanesulfonic acid, 10 μM EDTA, and 99.4 mM NaCl, pH 7.0] at 25 °C. Spectra were recorded at a drug concentration of 0.05 mM in the presence of 1 mM calf thymus DNA.

¹H NMR Assignments of the 5/d[(GAAGCTTC)]₂ Complex. The oligonucleotide d[(GAAGCTTC)]₂, synthesized by an automated DNA synthesizer at the Faculty of Pharmacy of Università di Napoli "Federico II", was a generous gift from Dr. Antonio Randazzo. Compound **5**, dissolved in D₂O/DMSO-*d*₆, 10:1, v/v, buffered at pH 7.0 (10 mM KH₂PO₄, 2 mM EDTA, and 70 mM KCl), was added in time to the octamer dissolved in the same solution. The solutions were degassed by argon. Spectra were recorded on a Bruker AMX 500 MHz spectrometer at 10 °C.

Computational Chemistry. Molecular modeling and graphics manipulations were performed using the SYBYL software package²² running on a Silicon Graphics R10000 workstation. Compound **5** was modeled using the TRIPOS force field³⁰ available within SYBYL, and its atomic charges were calculated using the semiempirical quantum mechanical AM1 method³¹ implemented in the MOPAC program.³² Energy minimizations and MD simulations of the 5/d[(GAAGCTTC)]₂ complex were realized by employing the AMBER program,³³ selecting the all-atom Cornell et al. force field.³⁴

(1) Model Building and Ligand Docking. The X-ray crystal structure of the DNA octamer [d(GAAGCTTC)]₂ complexed with N8-AMD (PDB entry code 209D, 3.0 Å resolution, *R* factor of 17.3%)⁸ was retrieved from the Brookhaven Data Bank.³⁵

A molecular model of compound **5** was constructed using standard bond lengths and bond angles of the SYBYL fragment library. The pyridine nitrogen of the ligand was taken as protonated, as it is at physiological pH. ESP-derived atomic partial charges were calculated using the AM1 Hamiltonian³¹

as implemented in MOPAC³² (CHARGE = +1; keywords ESP, PREC, GNORM = 0.001, EF).

Compound **5** was docked into the intercalation site of the DNA by superimposing it on N8-AMD. The relative orientation with respect to N8-AMD was derived by a straightforward fit of the common phenoxazine system. Subsequently, N8-AMD was removed from the site.

The 5/[d(GAAGCTTC)]₂ complex was then solvated in a periodic TIP3P water box³⁶ of dimensions 50 Å × 47 Å × 62 Å, which extended at least 10 Å from any solute atom. A total of 13 neutralizing counterions were added at the bifurcating positions of the O–P–O angle at a distance of 4.5 Å from the phosphorus atom.

(2) Molecular Dynamics Simulations. Energy minimizations and MD calculations were based on the all-atom Cornell et al. force field³⁴ available within the AMBER package, which was modified to include additional parameters for **5**. Most of these parameters were adapted by analogy from others included in the AMBER force field. Long-range interactions were treated using the particle mesh Ewald (PME) method.¹³ The PME charge grid spacing was about 1.0 Å, and the charge grid was interpolated using a cubic B-spline of the order of 4 with the direct sum tolerance of 0.000 01 at the 9 Å direct space cutoff. A constant temperature and pressure (300 K, 1 atm) was maintained throughout the simulations using the Berendsen scaling algorithm³⁷ with coupling constants of 0.2 ps in both cases. A time step of 0.002 ps was used to integrate the equations of motion with a nonbonded pairlist update frequency of 0.020 ps. All bonds involving hydrogen were constrained using the SHAKE algorithm.³⁸

Before beginning the "production-run" simulations, the following equilibration protocol was followed for relieving bad contacts between the solute and solvent and for allowing the reordering of water with minimal distortion to the starting structure. First, the water molecules and counterions in the periodic box were energy-minimized to an rms gradient of 0.0001, followed by 25 ps of MD with a simultaneous increase in temperature from 100 to 300 K. Subsequent 25 ps of MD and the final production runs were done by using the PME method to calculate electrostatic interactions. During this step, harmonic restraints of 500 kcal/mol were applied on 5/[d(GAAGCTTC)]₂ complex. Second, the whole system, including DNA, counterions, and waters, was subjected to 1000 steps of energy minimization followed by MD at 300 K for about 3 ps to remove close contacts and to relax the system. During this step, the restraints on DNA were reduced to 25 kcal/mol while the ligand was allowed to move. Last, external positional restraints on DNA were released in five steps by reducing the restraints by 5 kcal/mol per step followed by 600 steps of conjugate gradient minimization. Thus, in the fifth cycle, the whole system was minimized without harmonic restraints. After this, MD production runs of 70 ps were initiated after the system was heated from 100 to 300 K over 2 ps.

The CARNAL module of AMBER was used to check some structural properties (rmsd, hydrogen bonds). The hydrogen bond criterion was a maximum donor–acceptor distance of 3.5 Å and a minimum donor–proton–acceptor angle of 120°.

Acknowledgment. The authors thank the Centro Interdipartimentale di Metodologie Chimico-Fisiche and the Centro Interdipartimentale di Analisi Strumentale dell'Università di Napoli "Federico II". This work was supported by a grant from Ministero dell'Università e della Ricerca Scientifica.

References

- Butenandt, A.; Schäfer, W. Ommochromes. In *Recent Progress in the Chemistry of Natural and Synthetic Matters and Related Fields*; Gore, T. S., Yoshi, B. S., Suthankar, S. V., Tilak, B. D., Eds.; Academic Press: New York, 1962; pp 14–33.
- Bolognese, A.; Piscitelli, C.; Scherillo, G. Formation of Dihydrotriphendioxazines and Dihydroisotriphenodioxazines by Acidic Treatment of Some Substituted 3H-Phenoxazin-3-ones: Isolation and Characterization. A New Perspective in the Chemistry of Ommochromes. *J. Org. Chem.* **1983**, *48*, 3649–3652.

- (3) Ionescu, M.; Mantsch, H. Phenoxazine. *Adv. Heterocycl. Chem.* **1967**, *8*, 83–110.
- (4) Wakelin, L. P. G.; Waring, M. J. DNA Intercalating Agents. In *Comprehensive Medicinal Chemistry*; Sammes, P. G., Ed.; Pergamon Press: Oxford, U.K., 1990; Vol. 2, pp 703–724.
- (5) Kamitori, S.; Takusagawa, F. Crystal Structure of the 2:1 Complex Between d(GAAGCTTC) and the Anticancer Drug Actinomycin D. *J. Mol. Biol.* **1992**, *225*, 445–56.
- (6) Kamitori, S.; Takusagawa, F. Multiple Binding Modes of Anticancer Drug Actinomycin-D—X-ray, Molecular Modeling, and Spectroscopic Studies of D(GAAGCTTC)(2)—Actinomycin-D Complexes and Its Host DNA. *J. Am. Chem. Soc.* **1994**, *116*, 4154–4165.
- (7) Shinomiya, M.; Chu, W.; Carlson, R. G.; Weaver, R. F.; Takusagawa, F. Structural, Physical, and Biological Characteristics of RNA. DNA Binding Agent N8-Actinomycin D. *Biochemistry* **1995**, *34*, 8481–8491.
- (8) Takusagawa, F.; Takusagawa, K. T.; Carlson, R. G.; Weaver, R. F. Selectivity of F8-Actinomycin D for RNA:DNA Hybrids and Its Anti-Leukemia Activity. *Bioorg. Med. Chem.* **1997**, *5*, 1197–1207.
- (9) Meienhofer, I.; Atherton, E. *Structure—Activity Relationships among the Semisynthetic Antibiotics*; Perlman, D., Ed.; Academic Press: New York, 1977; pp 427–529.
- (10) Bolognese, A.; Scherillo, G.; Schäfer, W. Reaction of 2-Aminophenol and *p*-Benzoquinone in Acetic Acid. *J. Heterocycl. Chem.* **1986**, *23*, 1003–1006.
- (11) Nan'ya, S.; Maekawa, E.; Hayakawa, H.; Kitaguchi, Y.; Ueno, Y. Synthesis of 5*H*-Pyrido[2,3-*a*]phenoxazin-5-one and 5*H*-Pyrido[3,2-*a*]phenoxazin-5-one Derivatives. *J. Heterocycl. Chem.* **1985**, *22*, 1483–1485.
- (12) Ueno, Y. Synthesis of 5*H*-Pyridophenothiazin-5-ones. *Pharmazie* **1986**, *41*, 144.
- (13) Essmann, U.; Perera, L.; Berkowitz, M. L.; Darden, T.; Lee, H.; Pedersen, L. G. A Smooth Particle Mesh Ewald Method. *J. Chem. Phys.* **1995**, *103*, 8577–8593.
- (14) Pratt, Y. T. Quinolinquinones. VI. Reactions with Aromatic Amines. *J. Am. Chem. Soc.* **1962**, *27*, 3905–3910.
- (15) Fleming, I. *Frontier Orbitals and Organic Chemical Reactions*; John Wiley & Sons: Chichester, U.K., 1976.
- (16) Endicott, J. A.; Ling, V. The Biochemistry of P-Glycoprotein-Mediated Multidrug Resistance. *Annu. Rev. Biochem.* **1989**, *58*, 137–171.
- (17) Twentyman, P. R. Multidrug Resistance Strategy for Circumvention. *Drug News Perspect.* **1993**, *6*, 647–654.
- (18) Pastan, I.; Gottesman, M. M.; Ueda, K.; Lovelace, E.; Rutherford, A. V.; Willingham, M. C. A Retrovirus Carrying an MDR1 cDNA Confers Multidrug Resistance and Polarized Expression of P-Glycoprotein. *Proc. Natl. Acad. Sci. U.S.A.* **1988**, *85*, 4486–4490.
- (19) Chen, H. X.; Bamberger, U.; Heckel, A.; Guo, X.; Cheng, Y. C. BIBW 22, a Dipyridamole Analogue, Acts as Bifunctional Modulator on Tumor Cells by Influencing Both P-Glycoprotein and Nucleoside Transport. *Cancer Res.* **1993**, *53*, 1974–1977.
- (20) Gaj, C. L.; Anyanwutaku, I.; Chang, Y. H.; Cheng, Y. C. Decreased Drug Accumulation without Increased Drug Efflux in a Novel MRP-Overexpressing Multidrug-Resistant Cell Line. *Biochem. Pharmacol.* **1998**, *55*, 1199–1210.
- (21) Jones, R. L.; Wilson, W. D. Effects of Ionic Strength on the pK_a of Ligands Bound to DNA. *Biopolymers* **1981**, *20*, 141–154.
- (22) Misra, V. K.; Honig, B. On the Magnitude of the Electrostatic Contribution to Ligand–DNA Interactions. *Proc. Natl. Acad. Sci. U.S.A.* **1995**, *92*, 4691–4695.
- (23) SYBYL Molecular Modelling System, version 6.8; Tripos Inc.: St. Louis, MO.
- (24) Brooks, B. R.; Brucoleri, R. E.; Olafson, B. D.; States, D. J.; Swaminathan, S.; Karplus, M. CHARMM: A Program for Macromolecular Energy, Minimization and Dynamics Calculations. *J. Comput. Chem.* **1983**, *4*, 187–217.
- (25) Frisch, M. J.; Trucks, G. W.; Schlegel, H. B.; Scuseria, G. E.; Robb, M. A.; Cheeseman, J. R.; Zakrzewski, V. G.; Montgomery, J. A., Jr.; Stratmann, R. E.; Burant, J. C.; Dapprich, S.; Millam, J. M.; Daniels, A. D.; Kudin, K. N.; Strain, M. C.; Farkas, O.; Tomasi, J.; Barone, V.; Cossi, M.; Cammi, R.; Mennucci, B.; Pomelli, C.; Adamo, C.; Clifford, S.; Ochterski, J.; Petersson, G. A.; Ayala, P. Y.; Cui, Q.; Morokuma, K.; Malick, D. K.; Rabuck, A. D.; Raghavachari, K.; Foresman, J. B.; Cioslowski, J.; Ortiz, J. V.; Stefanov, B. B.; Liu, G.; Liashenko, A.; Piskorz, P.; Komaromi, I.; Gomperts, R.; Martin, R. L.; Fox, D. J.; Keith, T.; Al-Laham, M. A.; Peng, C. Y.; Nanayakkara, A.; Gonzalez, C.; Challacombe, M.; Gill, P. M. W.; Johnson, B. G.; Chen, W.; Wong, M. W.; Andres, J. L.; Head-Gordon, M.; Replogle, E. S.; Pople, J. A. *Gaussian 98*, revision A.10; Gaussian, Inc.: Pittsburgh, PA, 1998.
- (26) Adamo, C.; Barone, V. Toward Reliable Density Functional without Adjustable Parameters: The PBE0 Model. *J. Chem. Phys.* **1999**, *110*, 6158–6170.
- (27) Foresman, J. B.; Frisch, A. E. *Exploring Chemistry with Electronic Structure Methods*, 2nd ed.; Gaussian Inc.: Pittsburgh, PA, 1998.
- (28) Adamo, C.; Cassi, M.; Barone, V. An Accurate Density Functional Method for the Study of Magnetic Properties. The PBE0 Model. *THEOCHEM* **1999**, *493*, 145–157.
- (29) Adamo, C.; Cassi, M.; Rege, N.; Barone, V. In *New Computational Strategies for the Quantum Mechanical Study of Biological System in Condensed Phases, in Theoretical Biochemistry Processes and Properties of Biological Systems, Theoretical and Computational Chemistry*; Eriksson, L. A., Ed.; Elsevier Science B. D.: New York, 2001; Vol. 9, pp 467–538.
- (30) Vinter, J. G.; Davis, A.; Saunders, M. R. Strategic Approaches to Drug Design. 1. An Integrated Software Framework for Molecular Modelling. *J. Comput.-Aided Mol. Des.* **1987**, *1*, 31–55.
- (31) Dewar, M. J. S.; Zoebisch, E. G.; Healy, E. F.; Stewart, J. J. P. AM1: A New General Purpose Mechanical Molecular Model. *J. Am. Chem. Soc.* **1985**, *107*, 3902–3909.
- (32) MOPAC (version 6.0) is available from Quantum Chemistry Program Exchange, No. 455.
- (33) (a) Pearlman, D. A.; Case, D. A.; Caldwell, J. W.; Ross, W. S.; Cheatham, T. E., III; Debolt, S.; Ferguson, D. M.; Seibel, G. L.; Kollman, P. A. AMBER, a Package of Computer Programs for Applying Molecular Mechanics, Normal Mode Analysis, Molecular Dynamics and Free Energy Calculations To Simulate the Structural and Energetic Properties of Molecules. *Comput. Phys. Commun.* **1995**, *91*, 1–41. (b) Pearlman, D. A.; Case, D. A.; Caldwell, J. W.; Ross, W. S.; Cheatham, T. E., III; Ferguson, D. M.; Seibel, G.; Singh, U. C.; Weiner, P. K.; Kollman, P. A. AMBER, version 5.0; Department of Pharmaceutical Chemistry, University of California, San Francisco: San Francisco, CA, 1995.
- (34) Cornell, W. D.; Cieplak, P.; Bayly, C. I.; Gould, I. R.; Merz, K. M.; Ferguson, D. M.; Spellmeyer, D. C.; Fox, T.; Caldwell, J. W.; Kollman, P. A. A Second Generation Force Field for the Simulation of Proteins, Nucleic Acids, and Organic Molecules. *J. Am. Chem. Soc.* **1995**, *117*, 5179–5197.
- (35) Bernstein, F. C.; Koetzle, T. F.; Williams, G. J. B.; Meyer, E. F., Jr.; Brice, M. D.; Rodgers, J. R.; Kennard, O.; Shimanouchi, T.; Tasumi, T. The Protein Data Bank: A Computer Based Archival File for Macromolecular Structures. *J. Mol. Biol.* **1977**, *112*, 535–542.
- (36) Jorgensen, W. L.; Chandrasekhar, J.; Madura, J. D.; Impey, R.; W.; Klein, M. L. Comparison of Simple Potential Functions for Simulating Liquid Water. *J. Chem. Phys.* **1983**, *79*, 926–935.
- (37) Berendsen, H. J. C.; Postma, J. P. M.; van Gunsteren, W. F.; DiNola, A.; Haak, J. R. Molecular Dynamics with Coupling to an External Bath. *J. Chem. Phys.* **1984**, *81*, 3684–3690.
- (38) Ryckaert, J. P.; Ciccoti, G.; Berendsen, H. J. C. Numerical Integration of the Cartesian Equations of Motion of a System with Constraints: Molecular Dynamics of *n*-Alkanes. *J. Comput. Phys.* **1977**, *23*, 327–341.

JM020913Z